In Situ Compatibilization of Isotactic Polypropylene and High-Density Polyethylene by a Melt Cobranching Reaction

Jun Wang
Guizhou University
Le Yang
Guizhou University of Technology: Guizhou University
Xiaolong Li
Guizhou University
Zhu Luo (luozhu2000@sina.com)
Guizhou University https://orcid.org/0000-0001-8848-9354
Jianjun Li
Kingfa & Technological Co.,Ltd
Xiaosong Xia
Guizhou University
Changkai Linghu
Guizhou University

Research Article

Keywords: iPP, HDPE, long-chain branching copolymer, in situ compatibilization

Posted Date: March 30th, 2021

DOI: https://doi.org/10.21203/rs.3.rs-350514/v1

Version of Record: A version of this preprint was published at Journal of Polymers and the Environment on August 21st, 2021. See the published version at https://doi.org/10.1007/s10924-021-02263-7.

Abstract

Incompatible polypropylene (PP) and polyethylene (PE) are difficult to separate in mixed recycling streams such as waste plastic packaging, which makes these polyolefin mixtures unsuitable for high-quality products. In this work, based on the free radical branching reaction, a co-branching reaction of isotactic polypropylene (iPP) and high-density polyethylene (HDPE) blends was carried out in the presence of the peroxide, free radical regulator and multifunctional acrylate monomer, and a star-like long-chain branching (LCB) copolymer was acquired. The effect of in situ compatibilization on the structure and mechanical properties of iPP/HDPE was investigated, and the compatibilization mechanism was discussed. Results showed that the mechanical properties of the modified blends were largely improved, and efficient in-situ compatibilization of iPP and HDPE could be taken place in a wide process window. Moreover, the size of the dispersed phase in the modified blend was clearly decreased, and the interfacial thickness increased. Compared with the pure iPP/HDPE blend, the initial crystallization temperature of iPP in the modified iPP/HDPE blend was increased, and long branched chains of the LCB copolymer were physically entangled with the chemical identical homopolymers or even participate in the crystallization of iPP and HDPE. Thanks to the in situ compatibilization strategy, the compatibility of iPP/HDPE was significantly improved.

Introduction

As the main varieties of polyolefins, polyethylene (PE) and polypropylene (PP) account for approximately two-thirds of the global consumption of thermoplastic polymers [[i]]. However, the recycling rate of the polyolefin wastes in nature such as packaging is less than 10% [[ii]], which causes serious “white pollution”. Recent studies have reported that the harmful "microplastics" produced by discarded and buried plastics are widely found in water and organisms [[iii],[iv]]. PE and PP are incompatible nonpolar polyolefins and are usually mixed together in polyolefin wastes. Moreover, when plastic wastes are melt blended, the amorphous materials are usually enriched at the phase interface [2,[v]], which leads to a significant decrease in the compatibilizing effect of common compatibilizers such as short segment or random copolymers. The decline in the mechanical properties and processing properties of the hybrid PE/PP wastes restricts its high-quality reapplication, resulting in a low rate of recycling [[vi],[vii]]. Consequently, realizing the high-quality reuse of recycled polyolefin materials in a convenient way will help to improve the sustainability of polyolefin material applications.

In recent years, researchers have proposed many methods to solve this problem, including: recycling LDPE and PP through mechanical–chemical [[viii]]; making use of an alkylation reaction to improve the compatibility of PP/PE blends [[ix]]; using radiations [[x]] or peroxides [[xi]] to crosslink PP/PE blends; adding PE-g-PP graft copolymers [[xii]] or the nanoclay [[xiii]]. Recently, the high compatibilization efficiency of long block copolymers of ethylene and propylene is paid more attention to. In the research of Eagan et al. [1], long diblock and multiblock copolymers of ethylene and propylene synthesized by living polymerization were used as an adhesive layer between heterogeneous-grade PE and iPP laminates, and cocrystallization along the film interfaces or physical entanglement of the internal blocks with the

semicrystalline homopolymer lamellae at the interface was formed, which made PE and PP exhibited cohesive failure with the application of stress in the peel test. Therefore, the application of long block copolymer compatibilizers that can produce an interfacial "stitch" is an effective way to improve the recovery rate and reusability of polyolefin wastes [7,[xiv]]. Xu et al.[[xv]] found that long block copolymers replaced oligomers and impurities at the interface of the PE/PP blends, and only 0.2 wt % diblock copolymers could efficiently improve the interfacial adhesion. Furthermore, studies have shown [[xvi]] that adding 1.7 wt % synthetic comb copolymers can produce a significant compatibilization effect, which indicates that the compatibilization effect of the long-chain branched (LCB) copolymer is similar to that of the multiblock copolymer. Studies have also shown that the requirements of effective entanglement for PE/PP block copolymers are as follows: the PP block molecular weight is more than 2 times the entanglement molecular weight (PP entanglement molecular weight is approximately 5000 g/mol.), and the PE block molecular weight is more than 3 times the entanglement molecular weight (PE entanglement molecular weight is approximately 1000 g/mol.) [[xvii]]. If the block copolymer is required to form interphase co-crystals in the PE/PP blend, the requirements for molecular weights of the block copolymer are even larger[1].

However, the preparation of PE/PP long blocks and LCB copolymers are mainly through complex chemical synthesis [1,9,10] or polar group reaction [[xviii],[xix]] methods. Due to the low market value of recycled plastic materials, the application of expensive compatibilizers is restricted. Therefore, it is an economical and effective method to add a small amount of additives in the process of melting and mixing PE/PP wastes to generate long-chain copolymers in situ. Studies have shown that peroxides, free radical activity modifiers and trifunctional acrylate monomers could be used to prepare star-like LCB iPP or LCB HDPE [[xx],[xxi]]. Although PE and PP are immiscible polymers, they have good melt-mixability in the molten state [[xxii],[xxiii]], and maleic anhydride grafted PE and PP can be obtained simultaneously when the radical graft reaction occurs in the PE/PP blend [[xxiv]]. This result indicates that the probability of the reaction of monomeric radicals with macromolecular radicals of the two components is similar. Therefore, when the melt radical branching reaction system is applied to the iPP/PE blend, multifunctional monomers can be combined with different types of macromolecules to form a monomer-centric LCB copolymer, and the effect of an in situ high-efficiency compatibilization for PE/iPP blends can be produced.

In this work, iPP/HDPE blends in the presence of a small amount of peroxide initiator, multifunctional acrylate monomer and free radical regulator were melt blended to produce a LCB copolymer under different reaction times. Subsequently, the mechanical properties, compatibility, rheological behavior and crystallization behaviors of the blends were investigated, and the in situ compatibilization mechanism of the LCB copolymer on the blends was discussed.

Experimental Section

Materials. The isotactic polypropylene (iPP T30S, MFR=2.5 g/10 min at 230 °C with 2.16 kg) and high-density polyethylene (HDPE 5000S, MFR=1.7 g/10 min at 190 °C with 2.16 kg) in this work were both

obtained from Lanzhou Petrochemical Co., Ltd., China. 2, 5-Dimethyl-2, 5-di (tert-butylperoxy) hexane (DHBP) came from Aladdin-Aladdin Reagent Co., Ltd., China. Trifunctional trimethylolpropane triacrylate (TMPTA) was obtained from Liyang Runda Chemical Co., Ltd., China. Zinc dimethyldithiocarbamate (ZDMC) was purchased from Hebi Lianhe Chemical Co., Ltd. C., China. All reagents were used directly without further purification.

Preparation of the cobranched copolymers. The preparation of HDPE and iPP cobranched copolymers was carried out in a torque rheometer (XSM-500, Shanghai Kechuang Rubber & Plastic Machinery Co., Ltd., China). All the materials used in the reactive blending test were accurately weighed according to Table 1. Firstly, the DHBP and TMPTA were dissolved in an appropriate amount of acetone, and all of them were sprayed evenly on the already mixed HDPE and iPP. Then, ZDMC were added and mixed well. These samples were placed in an oven at 50 °C for 6 hours and then placed in the torque rheometer for mixing. During the mixing process, the rotor speed was 80 r/min and the temperature was 200 °C. The samples were taken at the reaction peak (about 140 s) and at the equilibrium point (about 220 s), which were used for the subsequent performance and structural tests. The above reaction products were cooled and then placed in a strong crusher. Finally, modified and pure pellets of the iPP/HDPE blends with a relatively uniform particle size were obtained.

Table 1. Formulation table for the modified component.

iPP(%)	HDPE(%)	DHBP (phr)	TMPTA(phr)	ZDMC(phr)
90	10	0.05	1.2	0.1
70	30	0.05	1.2	0.1
50	50	0.05	1.2	0.1
30	70	0.05	1.2	0.1
phr: mass parts of additives per 100 mass parts of polymer.				

Mechanical performance testing. The mechanical properties of the samples were tested using a CMT 6104 test machine (Meister Industrial Systems Co., Ltd., China). The pellets of the blends, pure iPP and HDPE were injection molded into standard samples using a PL860 injection molding machine (Wuxi Haitian Machinery Co., Ltd., China). The tensile properties, bending performances and notched impact strengths of the samples were tested according to ISO 1184-1983, ISO 178-2001 and ISO 180-2000, respectively. The test environment was at room temperature, and the average for each group was reported after being tested 5 times.

Scanning electron microscopy (SEM) analysis. After placing the samples in liquid nitrogen for 2 hours, the prenotched samples were quickly broken with an impact tester, and then the fracture surfaces of the samples were sprayed with gold. Finally, a scanning electron microscope (JEOL JSM-7500F, Japan) was

used to observe the surface of the impact section. The accelerating voltage was set to 5 kV, and the magnification was set to 1000 times.

Raman imaging technology analysis. The iPP/HDPE blend samples were analyzed with a laser confocal micro Raman DXR 2 spectrometer from American Thermo Fisher Co., Ltd. The notched samples were premade with a sharp blade and soaked in liquid nitrogen for 2 h before brittle fracture. The sections were frozen and flattened by the EMUC7 cryo-microtome of Leica, Germany, at -140 °C so that the section of the sample was smooth. Finally, the smooth section was analyzed with the Raman microscope.

Dynamic rheological analysis. This experiment used an ARES-G2 rotary rheometer from the American TA company for the rheology test in flat plate mode. The parallel plate diameter was 25 mm, and the upper and lower plate spacing was 1 mm. Firstly, a dynamic strain scan was performed to determine the linear viscoelastic range of the sample. The test temperature was 200 °C, and the strain was 1%. Then, a dynamic frequency sweep was performed in the linear viscoelastic region. The frequency sweep range was 0.05-500 rad/s.

Uniaxial elongation rheological characterization. Uniaxial elongation rheological characterizations were tested on a Haake Mars III rheometer (Thermo Fisher Scientific, USA) using the extensional viscosity fixture (EVF) at 200 °C under the nitrogen atmosphere. The strain rates in this test were 0.05 s^{-1} and 0.2 s^{-1}, respectively. The samples were hot-compressed into sheets with a width of 10mm and a thickness of 1mm for the uniaxial elongational viscosity tests. Before the rheological tests, all the samples were placed in the rheometer and heated for 5 min to completely melt the samples.

Thermal Analysis. Differential scanning calorimetry (DSC, TA-Q10, American) was utilized to study the crystallization and melting behavior of the iPP/HDPE samples. A sample (6-10 mg) was sealed in an aluminum pan and loaded in the DSC instrument. N_2 was used as the shielding gas, and the flow rate was set to 40 mL/min. The sample was quickly heated to 200 °C and kept at this temperature for 5 min to erase the previous thermal history before being cooled to 40 °C at a rate of 5 °C/min. The sample then underwent another heating cycle back to 200 °C at a rate of 5 °C/min. The crystallization and melting curves were recorded, and the reported peak crystallization (T_c) and melting temperatures (T_m) were obtained from the second heating cycles. In addition, the sample crystallinity (X_c) was calculated according to Formula 1:

$$\chi_c = \frac{\Delta H_m}{w_f \times \Delta H_m^{100\%}} \times 100\% \qquad 1$$

where $\Delta H^{100\%}_m$ was the theoretical melting enthalpy of iPP or PE with a crystallinity of 100%, and W_f was the mass fraction of iPP or PE in the blend. The values of $\Delta H^{100\%}_m$ for PE and iPP were 293 J/g and 207 J/g, respectively.

Polarized microscopy (POM) analysis. A small amount of sample was placed on the loaded piece, heated at 200 °C for 3 min to melt the sample, and then covered with a cover glass. During this period, a certain pressure was applied to make it into a film. The spherulite growth process of the sample was observed using an Axio Scoppe A1 polarizing microscope from the German ZEISS company. The temperature was increased to 200 °C at a heating rate of 20 °C/min, and the temperature was maintained for 5 min to eliminate the thermal history. Then, the temperature was decreased to 100 °C at a cooling rate of 2 °C/min to observe the growth process of the polymer spherulites.

Results And Discussion

Melt cobranching reaction process. Figure 1 shows the torque-time curves of the iPP, HDPE, pure and modified iPP/HDPE 90/10 blends and 70/30 blends. The first and second torque peaks on the curves correspond to the melting peaks of HDPE and iPP, respectively. During this period, the material in the barrel changes from a solid to a melt, accompanied by an increase and decrease in torque. The pure iPP/HDPE blend has only two melting peaks throughout the mixing time range, and the torque is almost constant when it is completely melted. However, a third peak appears in the curves of the cobranched samples, which are the branching reaction peak of iPP/HDPE.

Figure 2 is the mechanism of reaction process for the formation of the long-chain co-branched copolymer. First, the hydrogen atom on the methylene group in the HDPE molecular chain and the hydrogen atom on the tertiary carbon atom in the iPP molecular chain are easily seized by primary radicals produced by the decomposition of the organic peroxide and then the macromolecular radicals are produced. Moreover, multiple double bonds of the trifunctional acrylic monomer (M) are opened by the primary radicals to form monomer radicals. Then, these active monomer radicals are coupled with macromolecular radicals. Because a trifunctional acrylic monomer can be combined with different types of macromolecules, a cobranched structure centered on the trifunctional monomers is formed. However, iPP macromolecular tertiary carbon radicals are extremely unstable, which can easily cause a β-scission of the iPP molecular chain, and the methylene radicals of HDPE can easily combine with each other to produce a cross-linked structure. Therefore, the dithiocarbamate is added as a free radical activity regulator.

As shown in Figure 3 (taking iPP as an example), the dithiocarbamate can react with various active free radicals in the system, becoming a dithiocarbamoyl radical that does not have the ability to capture hydrogen (Process □). The reversible reactions of combining and separating occur between the generated dithiocarbamoyl radical and active radicals in the system [22], which decreases the instantaneous concentration of active radicals in the initial stage of the reaction. As the macromolecular free radicals in the system are continuously consumed in the branching reaction, the balance of the reversible reaction begins shifting to the reverse reaction, and the macromolecular radicals combined with the dithiocarbamoyl radicals are gradually released (process □), which extends the life of the macromolecular radicals, thereby promoting the branching reaction with multifunctional monomers and reducing the side reactions.

Mechanical performance testing. The mechanical properties of iPP, HDPE, pure and modified iPP/HDPE blends were tested, including the tensile properties, impact resistances and bending strengths of the materials. The results were listed in Table 2.

The tensile strength and rigidity of iPP are better than those of PE, but the impact toughness is poor; in contrast, PE has good impact toughness. Although the chemical structures of PE and iPP are similar, but because of the thermodynamically incompatible and difference in crystal structure, the mechanical properties of blends of HDPE and iPP are poor. It can be seen from Table 2 that compared with the pure blended samples, the overall mechanical properties of the cobranching modified samples are improved, especially the impact strength and elongation at break. For example, from Figure 4, the HDPE and iPP homopolymers are tough materials and their elongation at break are over 600%, however, the elongation at break of the pure iPP/HDPE 70/30 blend and 50/50 blend are just 75.2% and 123.3% respectively. Unexpectedly, the modified blends exhibit high toughness, and their elongation at break reaches 475.8% for iPP/HDPE 70/30 and 522.2% for iPP/HDPE 50/50. This result indicates that the introduction of a cobranched structure by chemical modification can significantly improve the compatibility of HDPE and iPP. And it can be seen from Figure 5, the modified iPP/HDPE 70/30 blend shows an obvious improvement in impact strength, but the improvement is not very significant. However, the modified samples of the iPP/HDPE 30/70 blend have approximately three times the impact strength of this pure blended sample. This is because improving the impact toughness of iPP dominant blends requires greater amounts of compatibilizer, when the more brittle iPP is the majority phase [25,26].

Table 2. Mechanical properties of iPP, HDPE, pure and modified iPP/HDPE blends.

Sample	Tensile (MPa)	Bending strength (MPa)	Notched impact strength ($kJ \cdot m^{-2}$)	Elongation at break (%)
iPP	36.3	42.1	3.9±0.13	680.3±35.6
HDPE	22.2	14.5	22.7±1.63	621.1±32.3
iPP/HDPE: 90/10	30.7	37.5	4.8±0.36	14.1±2.5
Modified[1] iPP/HDPE: 90/10	33.8	39.3	4.8±0.55	233.3±10.8
iPP/HDPE:70/30	30.2	31.1	4.8±0.24	75.2±5.7
Modified[1] iPP/HDPE: 70/30	31.1	30.1	9.8±1.12	475.8±28.2
Modified[2] iPP/HDPE: 70/30	31.1	33.7	10.7±1.25	361.2±31.5
iPP/HDPE: 50/50	26.6	24.9	6.1±0.98	123.3±10.3
Modified[1] iPP/HDPE: 50/50	27.6	27.2	23.1±1.95	522.2±37.4
Modified[2] iPP/HDPE: 50/50	25.6	26.4	24.6±2.19	480.5±34.6
iPP/HDPE: 30/70	24.2	21.9	12.8±1.23	195.5±18.5
Modified[1] iPP/HDPE: 30/70	24.6	22.6	35.5±4.52	450.6±43.6
Modified[2] iPP/HDPE:30/70	25.4	23.5	38.7±6.86	430.9±39.6
1: taken at the equilibrium point; 2: taken at the peak top				

Furthermore, From the data in Table 2, compared with the specimen taken at the equilibrium point, the impact strength of the specimen taken at the torque peak is slightly higher, but the elongation at break is slightly lower, and the overall performance difference is not obvious, which indicates that there is a wide process window for achieving an efficient in situ compatibilization of iPP and HDPE.

To observe the in situ compatibilization effect more intuitively, the appearance of tensile fracture specimen of iPP/HDPE 70/30 blends is shown in Figure 6. The severe delamination of the pure iPP/HDPE 70/30 blend can be seen during the tensile process, indicating its poor compatibility. In

contrast, the surface of the tensile deformed cobranching modified specimen is smooth and flat, indicating that a good in situ compatibilization effect has occurred.

Cryogenic fracture morphology. The notched samples were placed in a liquid nitrogen for 2 h and then immediately fractured using an impact test machine. Subsequently, the failure morphologies of the pure and unmodified HDPE/iPP 90/10 blends and 70/30 blends by imaging the fracture surface with SEM were investigated, as shown in Figure 7.

As shown in Figure 7a and 7b, which are the SEM images (magnified 1000 times) of the fracture of the pure iPP/HDPE 90/10 and 70/30 blends, the morphologies show an obvious gully, and the gully widens and deepens when the content of HDPE increases. This result is mainly due to the poor interfacial adhesion and interfacial strength, resulting in the phase interface breaking in the cryogenic fracture [27]. However, it can be observed from Figure 7c and 7d that the fracture morphologies of the modified iPP/HDPE 90/10 and 70/30 blends are uniform and smooth, indicating that interfacial adhesion of the iPP and HDPE phases is greatly improved after the cobranching modification.

Raman spectroscopy mapping. To detect the distribution of the two components in the iPP/HDPE blends, FT-Raman mapping was performed. The Raman spectra of the HDPE and iPP are shown in Figure 8a. The peak at 1295 cm^{-1} in the Raman spectrum of HDPE does not appear in the spectrum of iPP. This peak is the consecutive -CH_2 trans conformation peak in the crystalline polyethylene structure [28,29]. Therefore, we regard the Raman peak at 1295 cm^{-1} as the characteristic peak of the HDPE. The untreated Raman mapping images of the pure and modified iPP/HDPE 70/30 blends are shown in Figure 8b and 8c. The HDPE and iPP domains are denoted in the Raman mapping images as a red and green color, respectively. A yellow color appears at the interface, which is the area of mixed HDPE and iPP. For the modified sample, the size of the red domains decreases and the yellow area at the interface between two phases increases in the Raman mapping image, which means that the size of the dispersion phase of HDPE decreases and the interfacial thickness evidently increases. Because the Raman peak at 1295 cm^{-1} is the HDPE mark associated with a consecutive trans conformation, compared with the pure blend, many ordered or crystalline PE chains are present in the interfacial layer of the modified blend.

Dynamic rheological measurement. The van Gurp-Palmen (vGP) map can qualitatively reflect the molecular topological structure of the polymer. To eliminate the difference in molecular weight, molecular weight distribution and relaxation time of each sample, the complex modulus $|G^*|$ is normalized to the platform modulus G_N to obtain the reduced modulus G^*_{red}. Then, the reduced vGP map of each sample is obtained by plotting the phase angle δ against lgG^*_{red}. Figure 9a shows that iPP exhibits clearly linear polymer characteristics, and its δ monotonically decreases with an increasing G^*_{red} in the test range. Although the curve of the pure iPP/HDPE blend shows a small fluctuation, the overall monotonic decrease is obvious, and there is no obvious inflection point. This result is caused by the relaxation of the dispersed phase of the system and the existence of the phase interface [30]. An obvious inflection point can be seen on the vGP curve of the modified samples, which corresponds to the relaxation process of

the long-chain branch in the samples. Liu et al. [31] studied the vGP maps of various branched polyethylenes and produced a topology map based on them. As seen from Figure 9a, the curves of the modified sample exhibits a "bump" shape after the inflection point, indicating that the samples contain a typical star-like branched structure [33,32,33]. Moreover, the inflection point of the modified sample taken at the equilibrium point is earlier than the inflection point of the modified sample taken at the top of the reaction peak, which indicates that the modified cobranched material exhibits characteristics of a more stable star-like LCB structure with the extension of reaction time [34,35].

Comparing with the dynamic shear rheology, elongational rheology is more sensitive to the branched molecular structure. The evaluation of the strain-hardening behavior of melt in elongational flow can be used to confirm the existence of long chains branched molecular structure in the iPP/HDPE blend [36]. The transient elongational viscosities of pure and modified iPP/HDPE 70/30 blends at different strain rates are showed in Figure 9b. It can be seen that the transient elongational viscosities of pure iPP/HDPE 70/30 blends increase with time at the beginning of stretching, but decrease before the end of the tests, which is so-called strain-softening behavior [37]. This trend indicates a lack of branched chains in pure iPP/HDPE 70/30 blends due to their linear molecular structure. On the contrary, the strain-hardening behavior is evident in modified samples, and this behavior is more obvious at low rates. The remarkable strain hardening behavior confirms the long branched molecular structure in the modified iPP/HDPE 70/30 blend. Therefore, similar to the bimodal P(E-cb-P) comb block, the remarkable strain hardening observed in modified blends may arise from the increases in the blend interfacial area and the entanglement of the branched chains of LCB copolymers within the homopolymer phases [38].

Analysis of the crystallization behavior. Differential scanning calorimetry (DSC) was performed on the iPP, HDPE, pure and modified iPP/HDPE blends. The results are shown in Figure 10, and the onset temperature of crystallization and the crystallinity calculated from the melting curves are listed in Table 3.

In Figure 10a, the crystallization temperature of iPP is clearly higher than that of HDPE, and the crystallization temperature ranges of iPP and PE partly overlap with each other. As shown in Table 3, the crystallinities of iPP and HDPE are 45.63% and 59.39%, respectively. iPP and HDPE components in the pure blends crystallize separately in their own cells; thus iPP and HDPE components in the melt blends repel each other and form separated phase structures in the crystallization process. This mechanism results in a decrease in crystallinity. Figure 10c, 10e and Table 3 show that the initial crystallization temperature of iPP in the modified iPP/HDPE blend increases. This phenomenon is mainly because the long-chain cobranched structure are easily discharged into the crystal lattice and play a role in nucleation, which promotes the increase in the initial crystallization temperature of the modified iPP/HDPE blend. On the other hand, the regularity of the polymer structure is destroyed by cobranched structures [39], which decreases the degree of crystal perfection and results in a wide crystallization temperature range.

Table 3. Crystallinity and onset crystallization temperature of HDPE, iPP and iPP/HDPE blends.

Sample	Crystallinity of iPP/HDPE(%)	Crystallization onset temperature of iPP/HDPE (°C)
HDPE	0/59.39	0/120.28
iPP	45.63/0	124.63/0
Pure iPP/HDPE: 70/30	29.99/53.03	126.21/120.00
Modified[1] iPP/HDPE: 70/30	33.71/47.07	135.33/120.75
Modified[2] iPP/HDPE: 70/30	32.89/44.50	132.61/119.96
Pure iPP/HDPE: 30/70	24.30/49.24	125.5/119.93
Modified[1] iPP/HDPE: 30/70	22.60/51.59	133.08/121.84
Modified[2] iPP/HDPE: 30/70	15.83/42.94	134.00/121.49
1: taken at the equilibrium point; 2: taken at the peak top		

In addition, the crystallinity of the modified blends taken at the peak top is lower than that of the modified blends taken at the equilibrium point in Table 3, which means that the main chain regularity of the polymers becomes better with the extension of blending time. Therefore, the degree of branching does not increase after the branching reaction peak in the melt modification process. As shown in Figure 10e, when the content of iPP is low in the pure blend, the steric hindrance effect of HDPE causes the iPP crystallization undercooling to increase, and only a single peak almost appears in the cooling curve. However, the LCB copolymer distributed at the interface of iPP and HDPE in the modified blend [16] can release its propylene chain into the iPP lattice; thus the steric hindrance effect of PE decreases, and the crystallization of iPP is completed before the crystallization of PE.

To further investigate the crystallization behavior of the samples, the spherulite growth processes of the pure and modified iPP/HDPE 70/30 blends were observed using a polarizing microscope. The pure iPP/HDPE blend and the modified sample taken at the equilibrium point were cooled at a rate of 2 °C/min starting at 200 °C, and the spherulite growth process was observed (photographed every 60 s). According to the initial crystallization temperature of different samples in Table 3, the polarizing microscopy pictures at different temperatures were selected, and these are shown in Figure 11 and 12.

As shown in Figure 11, for the pure iPP/HDPE blend, the mutual restriction between the two components makes the spherulites obviously incomplete, and it is worth noting that the initial crystallized iPP spherulites cannot enter the PE domains indicated by the arrows. The reason for this behavior is that the first crystallized iPP constantly repels the melted PE with an increasing spherulite size. After the

temperature drops to a certain level, the PE phase nucleates and crystallizes by itself, thus forming a sea-island structure.

As shown in Figure 12, for the modified iPP/HDPE blend, the spherulites are complete and grow continuously. An obvious phase boundary cannot be found, and the spherulites of the later crystallized HDPE indicated by the arrows in the Figure 12 are intertwined with those of iPP. Furthermore, different from the dense spherulites in Figure 11, obvious gaps between the lamellae inside the spherulites can be seen in Figure 12. This result is mainly because spherulites are composed of radially growing lamellae, and when a part of the branch chains of the branched copolymer cocrystallize with the chemical identical homopolymer, another kind of branch chains cannot enter the crystal lattice and is retained between the lamellae, which leads to the formation of the obvious gaps between the lamellae inside the spherulites. It is speculated that the ethylene and propylene molecular chains of the cobranched copolymer enriched at the interface of HDPE and iPP participate in the crystallization of HDPE and iPP, respectively, thereby decreasing the restriction effect between the two components.

Compatibility mechanism models. To facilitate a better understanding of the role of the LCB copolymer between the HDPE and iPP crystals, we made the schematic diagram, as shown in Figure 13. The chains and spherulites of HDPE and iPP are shown in different colors to facilitate identification.

As seen from Figure 13, the cobranched copolymers enrich on the interface of the different kinds of spherulites, which produce microphase separation and the formation of ordered structures, and the branched chain of LCB copolymers participate in the crystallization of chemical identical homopolymer spherulites. In addition, some of the cobranched copolymers are concentrated in the gap between the lamellae in the homopolymer spherulites, which exist mainly in the amorphous state due to the limit of the molecular chain motion, and a part of their chemical identical branched chains participate in crystallization of the homopolymer spherulites.

Summary And Conclusions

A cobranched reaction system composed of iPP/HDPE blends in the presence of the peroxide, free radical regulator and polyfunctional acrylate monomer was used to synthesize LCB copolymers in situ for the efficient compatibilization of iPP/HDPE blends in an economical and convenient manner. The star-like cobranched molecular structure was formed in situ in the melt blending and the strain-hardening behavior is evident in modified samples. The comprehensive mechanical properties of the modified blend were significantly improved. For example, compared with the pure iPP/HDPE 50/50 blend, the elongation at break of the modified samples was increased by over 4 times and the notched impact strength was increased by approximately 4 times. In addition, for the modified blends with the same composition but different blending times, the difference in the overall performance was not obvious, which indicated that there was a wide process window for the efficient in situ compatibilization of iPP and HDPE. As a result, the size of the dispersed phase in the modified blend clearly decreased while the interfacial thickness increased. The initial crystallization temperature of iPP in the modified iPP/HDPE blend was increased by

the nucleation effect of the long-chain branches. Furthermore, compared with the incomplete spherulites and clearly separated phase structures of the pure iPP/HDPE blend, the spherulites of the modified iPP/HDPE blend were complete and grew continuously, which was due to LCB copolymer participating in the crystallization of HDPE and iPP, making these two crystallizations almost simultaneously. The long branched chain LCB copolymers at the interface of the two phases entangled with iPP and HDPE at the interface of the two phases and were even involved in the crystallization of iPP and HDPE, which significantly improved the compatibility of iPP and HDPE.

Our work offers a novel approach to solve the current bottleneck for the low-cost compatibilization of the mixture of polyolefin wastes and short the reapplication cycle.

Declarations

Acknowledgments

This study was funded by the National Key R & D Plan of China (2019YFC1908200).

Conflict of Interest

The authors declare that they have no conflict of interest.

References

1 . Eagan JM, Xu J, Girolam RD, Christopher MT, Christopher WM, Anne ML, Frank SB, Geoffrey WC (2017) Combining polyethylene and polypropylene: Enhanced performance with PE/iPP multiblock. Science 355:814-816.

2 . Jordan AM, Kim K, Soetrisno D, Hannah J, Bates FS, Jaffer SA, Lhost O, Macosko CW (2018) Role of crystallization on polyolefin interfaces: an improved outlook for polyolefin blends. Macromolecules 51:2506-2516.

3 . Herbort AF et al (2018) Alkoxy-silyl induced agglomeration: a new approach for the sustainable removal of microplastic from aquatic systems. J Polym Environ 26:4258–4270

4 . Rochman CM (2018) Microplastics research—from sink to source. Science 360:28-29.

5 . Chaffin KA, Knutsen JS, Brant P, Bates FS (2000) Highstrength welds in metallocene polypropylene/polyethylene laminates. Science 288:2187-2190.

6 . Yasamin K, Ramezani KA, Denis R (2015) Compatibilization efficiency in post-consumer recycled polyethylene/polypropylene blends: Effect of contamination. Polym Eng Sci 55:2368-2376.

7 . Creton C (2017) Molecular stitches for enhanced recycling of packaging. Science 355:797-798.

8 . Camargo R D, Saron C (2020) Mechanical-Chemical Recycling of Low-Density Polyethylene Waste with Polypropylene. J Polym Environ 28(3):794-802.

9 . Carvalho VL, Safieddine C, Demarquette NR, Pinheiro LA (2019) In situ compatibilization of a polyethylene, polypropylene, and polystyrene ternary blend through Friedel–Crafts alkylation. J Appl Polym Sci 137:48295.

10 . Wang WZ, Zhang XC, Maoc ZY, Zhao WQ (2019) Effects of gamma radiation on the impact strength of polypropylene (PP)/high density polyethylene (HDPE) blends. Results Phys 12:2169-2174.

11 . Gu JQ, Xu HY, Wu CF (2013) The Effect of PP and Peroxide on the Properties and Morphology of HDPE and HDPE/PP Blends. Adv Polym Tech 32:72-72.

12 . Klimovica K, Pan SS, Lin TW, Peng, XY, J Ellison C, M LaPointe A, S Bates F, W Coates G (2020) Compatibilization of iPP/HDPE Blends with PE-g-iPP Graft Copolymers. Acs Macro Lett 9:1161-1166.

13 . Mohan TP Kanny K, (2013) Melt blend studies of nanoclay-filled polypropylene (PP)–high-density polyethylene (HDPE) composites. J Mater Sci 48(23):8292-8301

14 . Jeannette MG, Megan LR (2017) The future of plastics recycling. Science 358:870-872.

15 . Xu J, Eagan JM, Kim SS, Pan SS, Lee, BJ, Klimovica K, Jin KL, Lin TW, Micah JH, Ellison CJ, LaPointe AM, Coates GW, Bates FS, (2018) Compatibilization of isotactic polypropylene (iPP) and high-density polyethylene (HDPE) with iPP–PE multiblock copolymers. Macromolecules 51:8585-8596.

16 . López-Barrón, Carlos R, Tsou AH (2017) Strain hardening of polyethylene /polypropylene blends via interfacial reinforcement with poly(ethylene-cb-propylene) comb block copolymers. Macromolecules 50:2986-2995.

17 . Chaffin KA, Bates FS, Brant P, Brown GM, (2000) Semicrystalline blends of polyethylene and isotactic polypropylene: improving mechanical performance by enhancing the interfacial structure. J Polym Sci Pol Phys 38:108-121.

18 . Li YC, Jia S, Dua SL, Wang YF, Lu LD, Zhang JB (2018) Improved properties of recycled polypropylene by introducing the long chain branched structure through reactive extrusion. Waste Manage 76:172-179.

19 . Yao Z, Lu ZQ, Zhao X, Qu BW, Shen ZC, Cao K (2009) Synthesis and characterization of High-Density Polypropylene-grafted polyethylene via a macromolecular reaction and its rheological behavior. J Appl Polym Sci 111:2553-2561.

20 . Li Y, Yao Z, Chen ZH, Qiu SL, Zeng CC, Cao K (2015) High melt strength polypropylene by ionic modification: Preparation, rheological properties and foaming behaviors Polymer. 70:207-214.

21 . Liu JY, Yu W, Zhou CX (2011) Polymer chain topological map as determined by linear viscoelasticity. J Rheol 55:545-570.

22 . Zhang ZJ, Xing HP, Qiu J, Jiang ZW, Yu HO, Du XH, Wang YH, Ma L, Tang T (2010) Controlling melt reactions during preparing long chain branched polypropylene using copper N, N-dimethyldithiocarbamate. Polymer 51:1593-1598.

23 . Li SZ, Xiao MM, Guan Y, Wei DF, Xiao HN, Zheng NN (2012) A novel strategy for the preparation of long chain branching polypropylene and the investigation on foamability and rheology. Eur Polym J 48:362-371.

24 . Münstedt H, Schwarzl FR (2011) Rheological properties and molecular structure of polymer melts. Soft Matter 7:2273-2283.

25 . Blom HP, Teh JW, Rudin A (1996) iPP/HDPE blends II Modification with EPDM and EVA. J Appl Polym Sci 60:1405-1417.

26 . Ha MH, Kim BK, Kim EY (2004) Effects of Dispersed Phase Composition on Thermoplastic Polyolefins. J Appl Polym Sci 93:179–188.

27 . Zhang C , Yi XS, Asai S, Sumita M (2000) Morphology, crystallization and melting behaviors of isotactic polypropylene/high density polyethylene blend: effect of the addition of short carbon fiber. J Mater Sci 35:673-683.

28 . Prokhorov KA, Nikolaeva GY, Sagitova EA, Pashinin PP, Guseva MA, Shklyaruk BF, Gerasin VA (2018) Raman structural study of melt-mixed blends of isotactic polypropylene with polyethylene of various densities. Laser Phys 28:045702

29 . Samuel A Z (2020) Direct estimation of polymer crystallinity with Raman spectroscopy using ratio of scattering cross-sections estimated from variable temperature measurements. Spectrochim Acta A 224:117431.

30 . Wu DF, Zhang YS, Zhang M, Wu LF (2007) Morphology, nonisothermal crystallization behavior, and kinetics of poly(phenylene sulfide)/polycarbonate blend. J Appl Polym Sci 105:739-748.

31 . Liu J, Yu W, Zhou C (2011) Polymer chain topological map as determined by linear viscoelasticity. J Rheol 55:545-570.

32 . Kempf M, Ahirwal D, Cziep M, Wilhelm M (2013) Synthesis and Linear and Nonlinear Melt Rheology of Well-Defined Comb Architectures of PS and PpMS with a Low and Controlled Degree of Long-Chain Branching. Macromolecules 46:4978-4994.

33 . Lohse DJ, Milner ST, Fetters LJ, Xenidou M, Hadjichristidis N, Mendelson R (2002) A Well-defined, model long chain branched polyethylene 2 Melt rheological behavior. Macromolecules 35:3066-3075.

34 . Trinkle S, Friedrich C (2001) Van Gurp-Palmen-plot: a way to characterize polydispersity of linear polymers Rheol Acta 40:322-328.

35 . Kanso MA, Giacomin AJ (2020) Van Gurp–Palmen relations for long-chain branching from general rigid bead-rod theory. Phys Fluids 32:033101.

36 . Stadler FJ, Chun YS, Han JH, Lee E, Park SH, Yang CB, Choi C (2016) Deriving comprehensive structural information on long-chain branched polyethylenes from analysis of thermos-rheological complexity. Polymer 104:179-192.

37 . López-Barrón C, Patrick B, Maksim S, Lu JM, Kang SH, Throckmorton J, Trent M, Truyen P, Rebecca C (2018) Long-chain hyperbranched comb block copolymers: synthesis, microstructure, rheology, and thermal behavior. Macromolecules 51:5720-5731.

38 . Tsou AH, López-Barrón, Carlos R, Jiang P, Crowther, DJ, Zeng Y (2016). Bimodal poly(ethylene-cb-propylene) comb block copolymers from serial reactors: synthesis and applications as processability additives and blend compatibilizers. Polymer 104:72-82.

39 . Tian Z, Chen KR, Liu BP, Luo N, Du WL, Qian F (2015) Short-chain branching distribution oriented model development for Borstar bimodal polyethylene process and its correlation with product performance of slow crack growth. Chem Eng Sci 130:41-55.

Figures

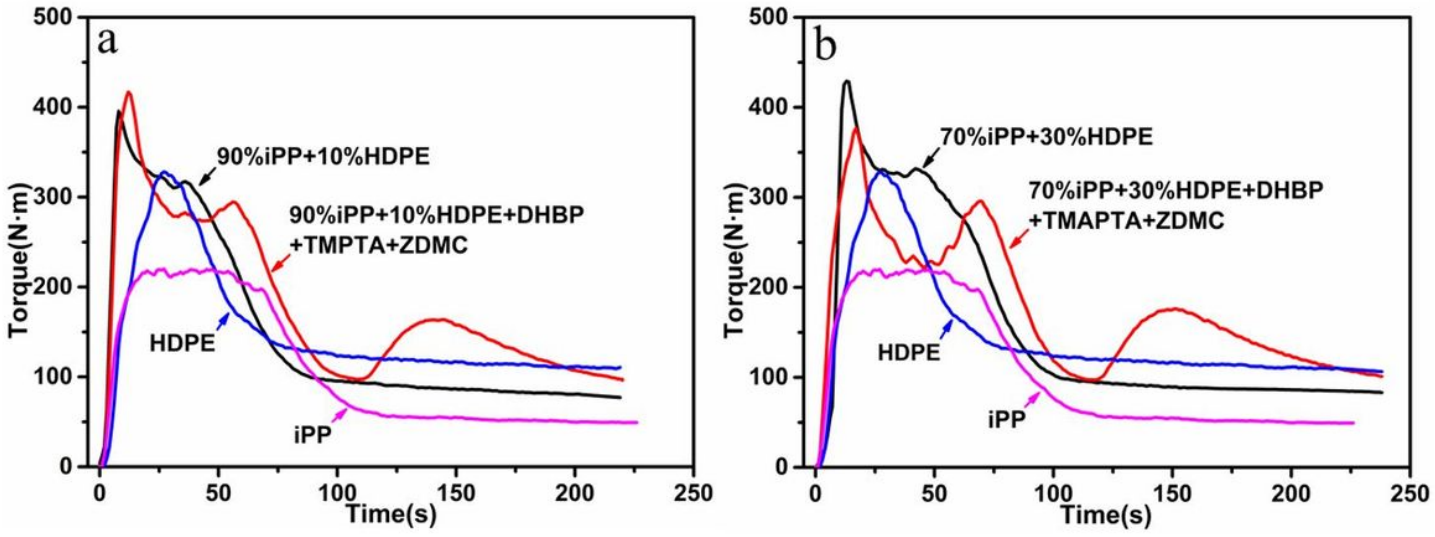

Figure 1

Torque-time curves of HDPE, iPP, pure and modified iPP/HDPE blends. (a: HDPE, iPP and the iPP/HDPE 90/10 blend; b: HDPE, iPP and the iPP/HDPE 70/30 blend.)

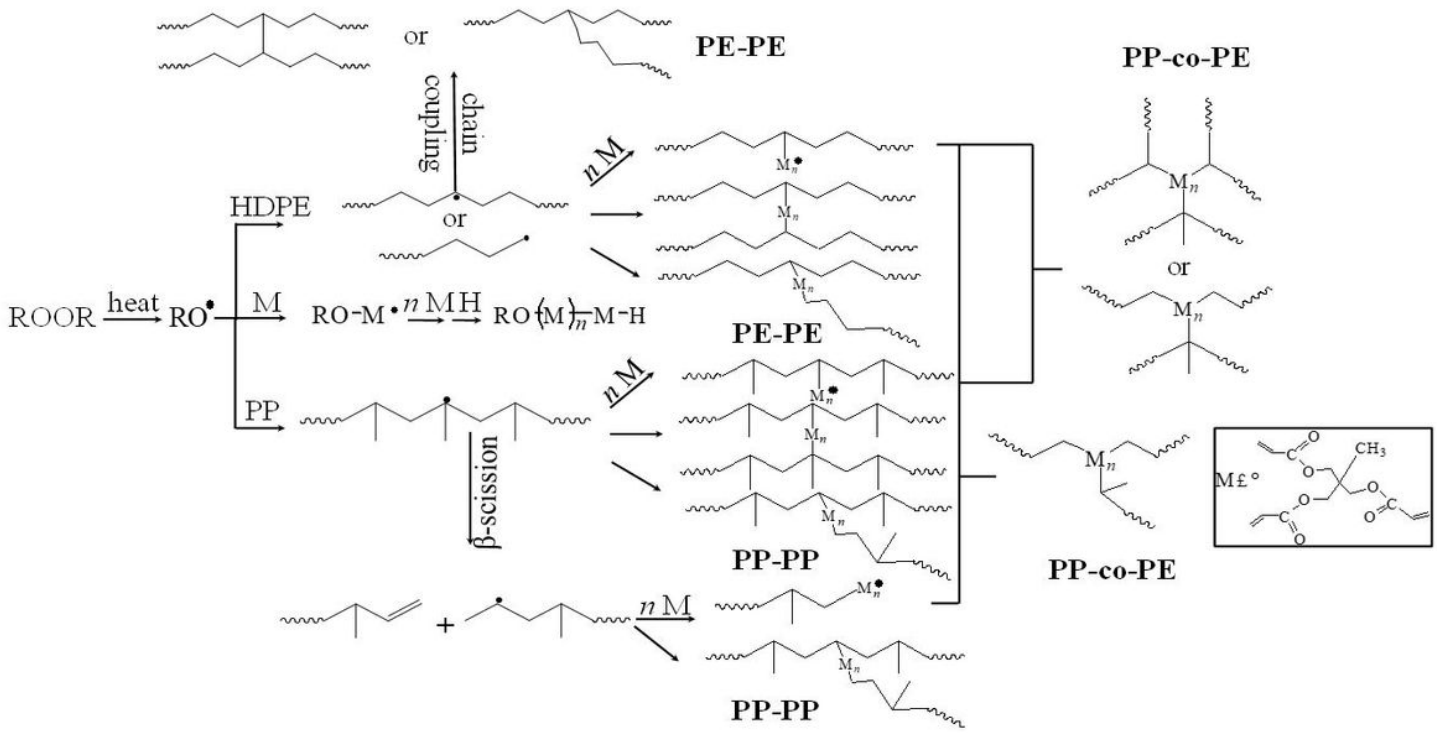

Figure 2

Schematic diagram of the co-branching reaction of iPP/HDPE.

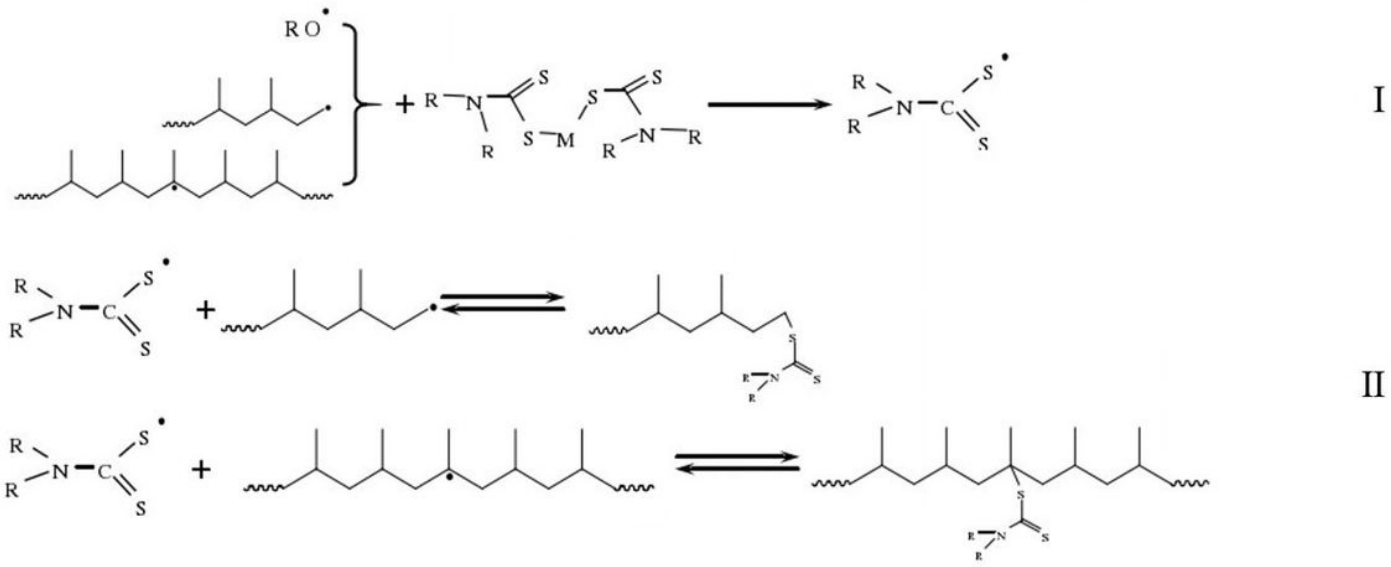

Figure 3

Mechanism of action of free radical activity regulators.

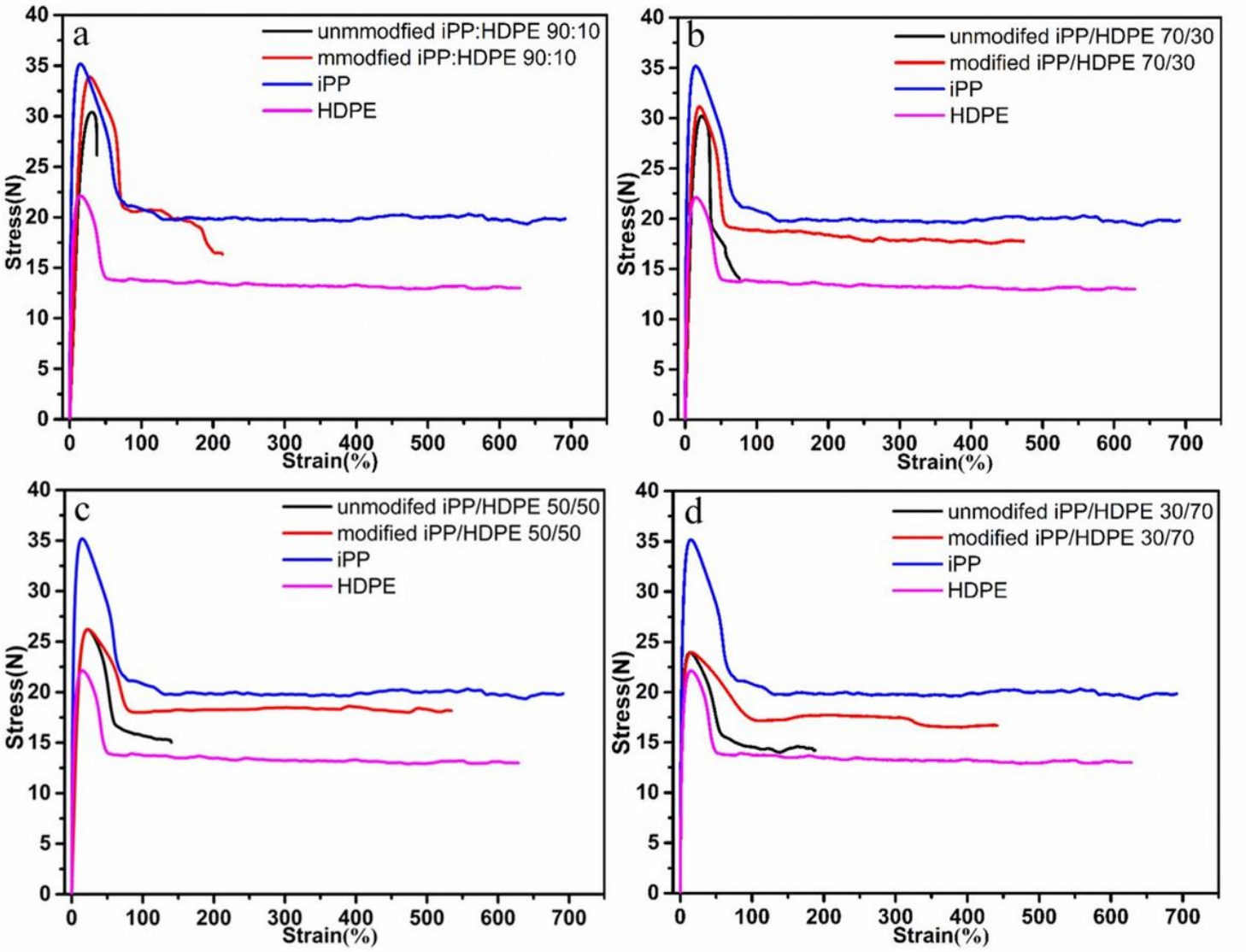

Figure 4

Stress-strain curves of iPP, HDPE, and iPP/HDPE blends (a: iPP/HDPE 90/10 blends; b: iPP/HDPE 70/30 blends; c: iPP/HDPE 50/50 blends; d: iPP/HDPE 30/70 blends).

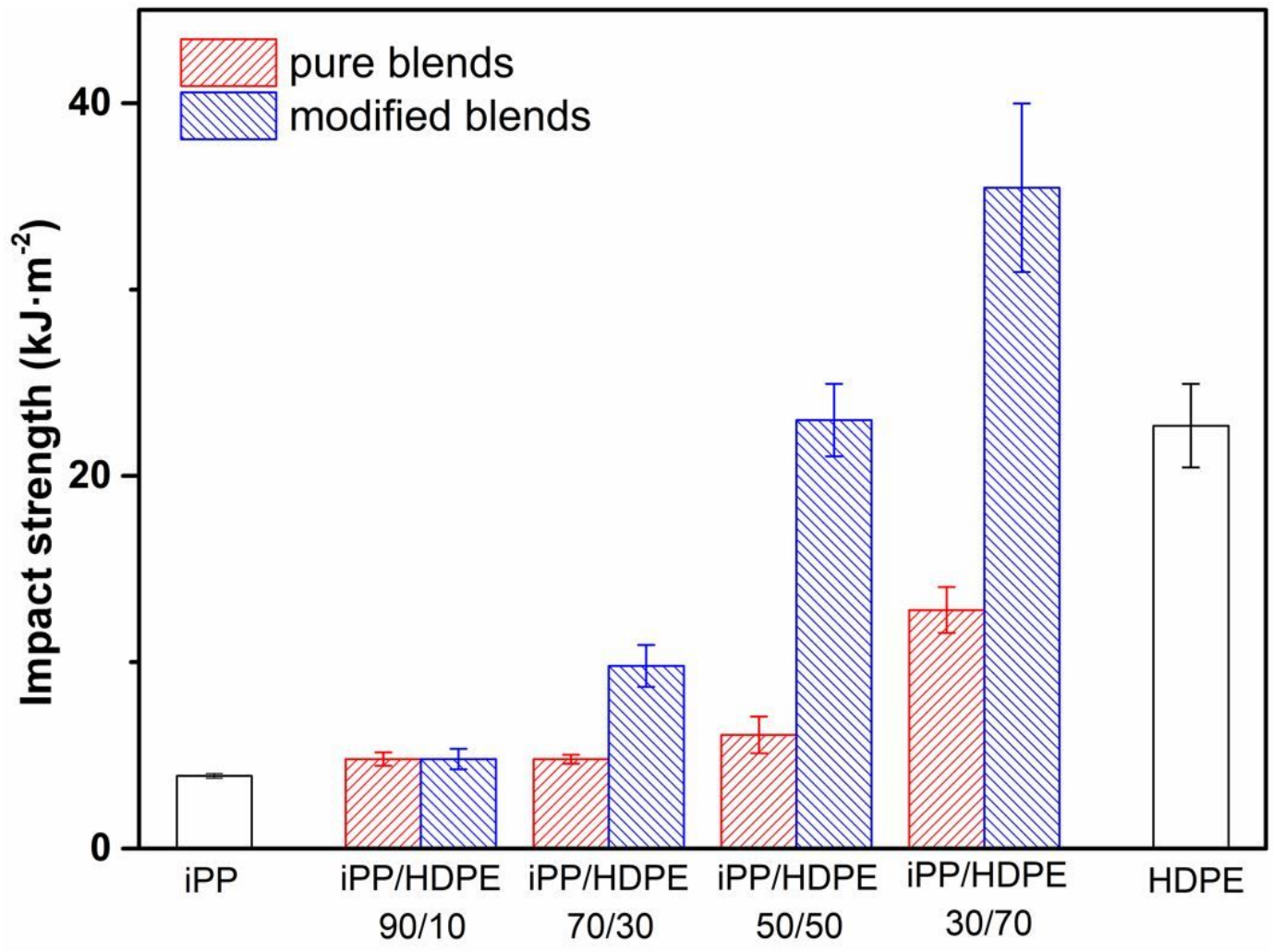

Figure 5

Notched impact strength of iPP, HDPE, pure and modified iPP/HDPE blends taken at an equilibrium point.

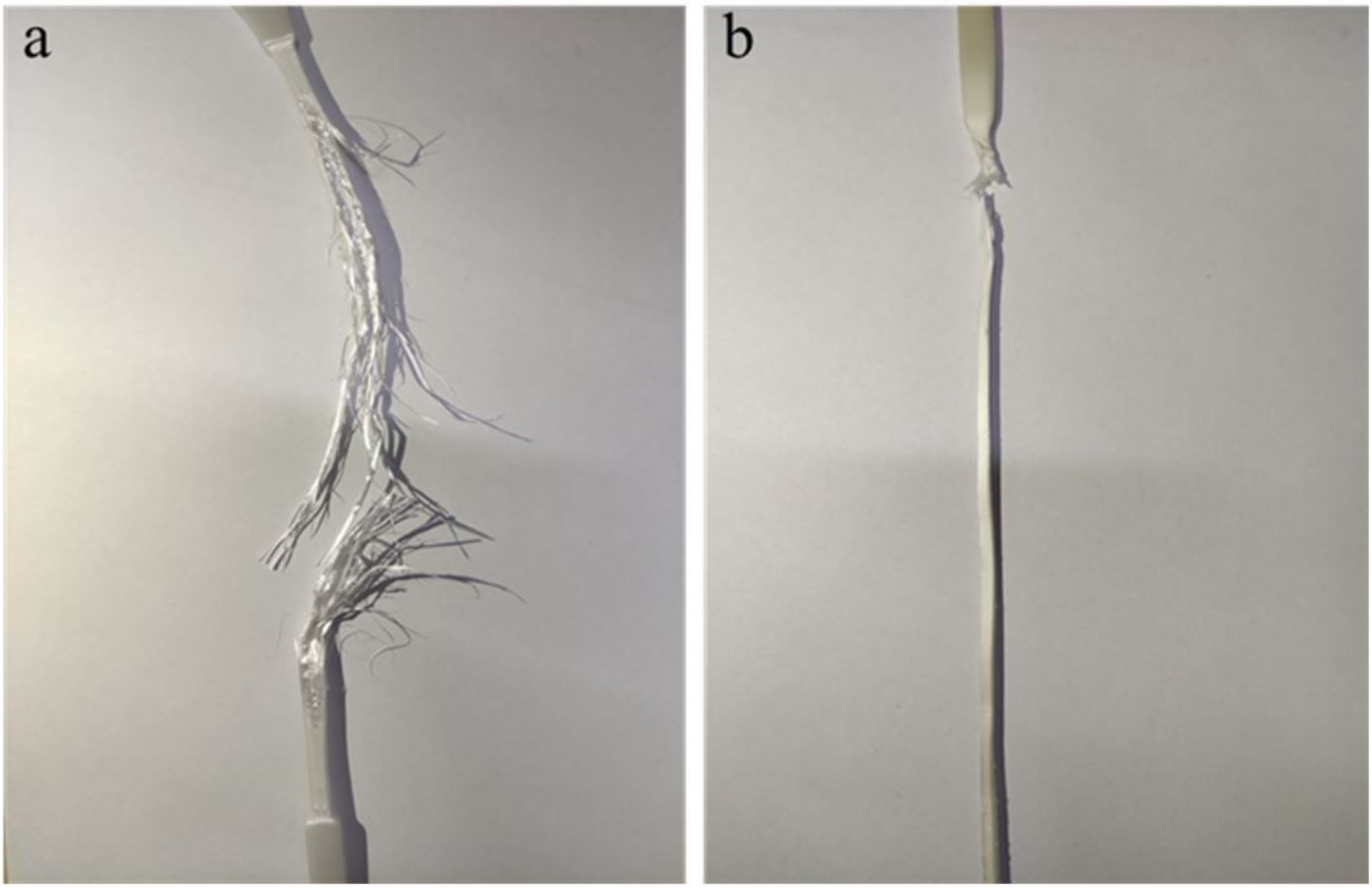

Figure 6

Tensile specimens of pure and modified iPP/HDPE 70/30 blends (a, the pure iPP/HDPE 70/30 blend; b, the modified iPP/HDPE 70/30 blend).

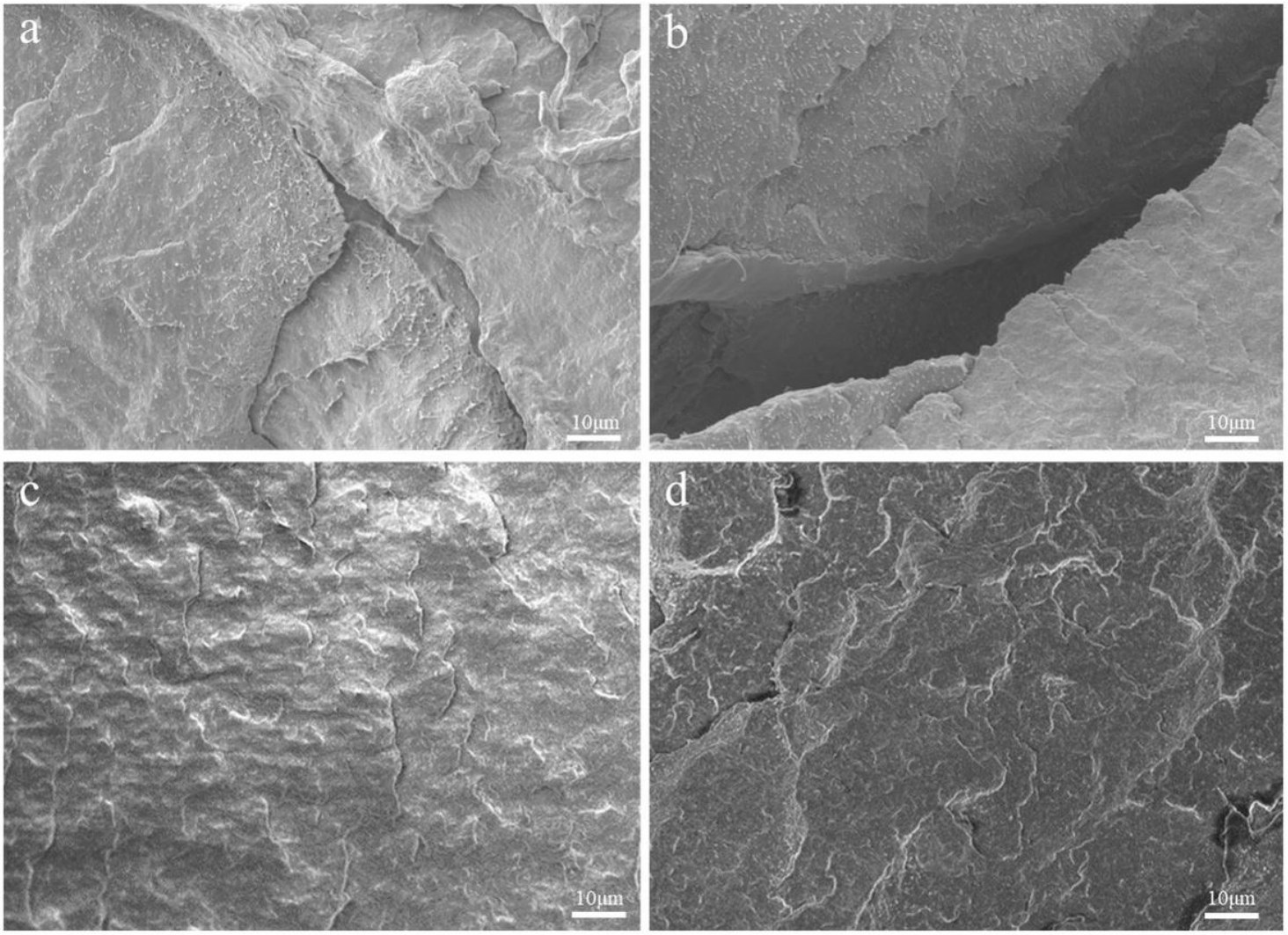

Figure 7

SEM image of pure and modified iPP/HDPE blends cryogenic fracture. (a, c: the cryogenic fracture morphologies of pure and modified iPP/HDPE 90/10 blends; b, d: the cryogenic fracture morphologies of pure and modified iPP/HDPE 70/30 blends.)

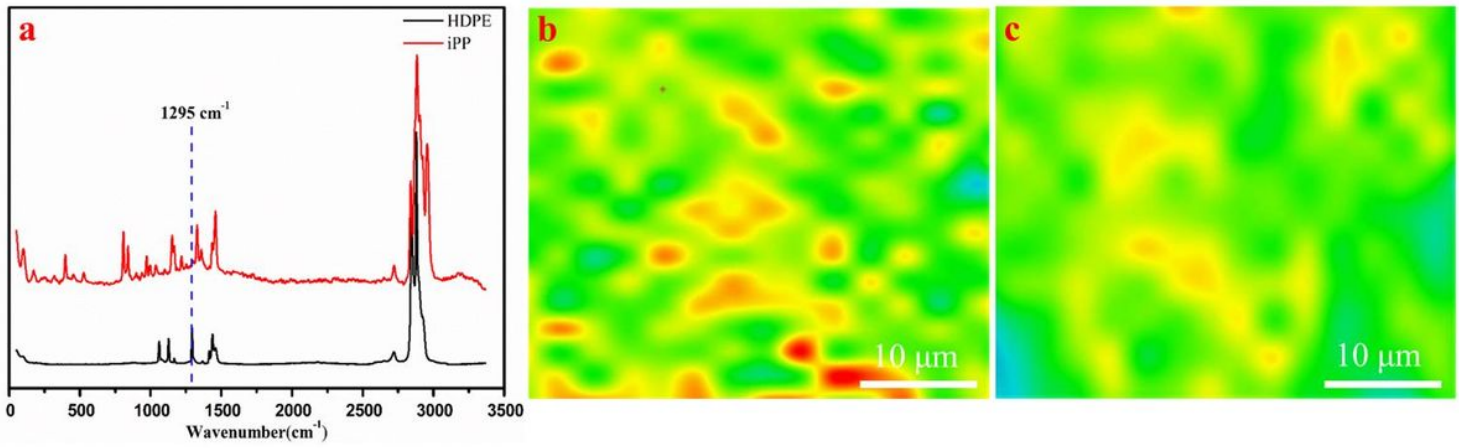

Figure 8

(a) Raman spectra of HDPE and iPP in the wavenumber region of 0~3400 cm-1; (b, c) Raman mapping images of pure and modified iPP/HDPE 70/30 blends (Red represents the distribution of HDPE in the blend.).

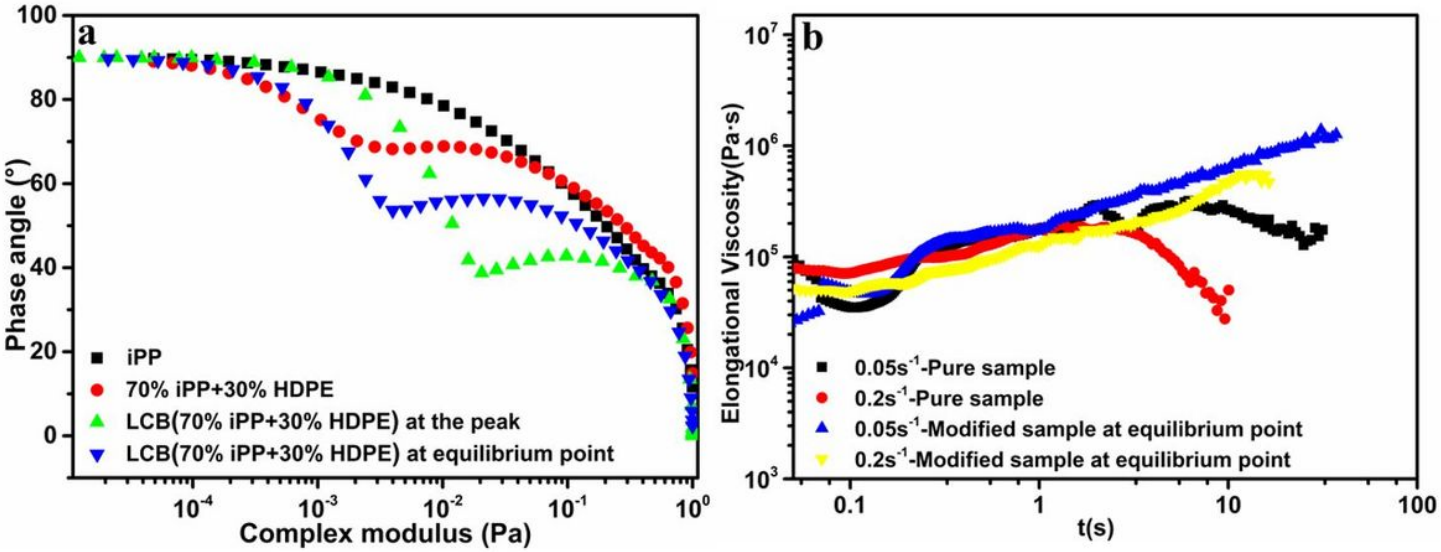

Figure 9

a: Van Gurp-Palmen plots of iPP, pure and modified iPP/HDPE 70/30 blends; b: Transient elongational viscosity versus a time of pure and modified iPP/HDPE 70/30 blends at different elongational rates.

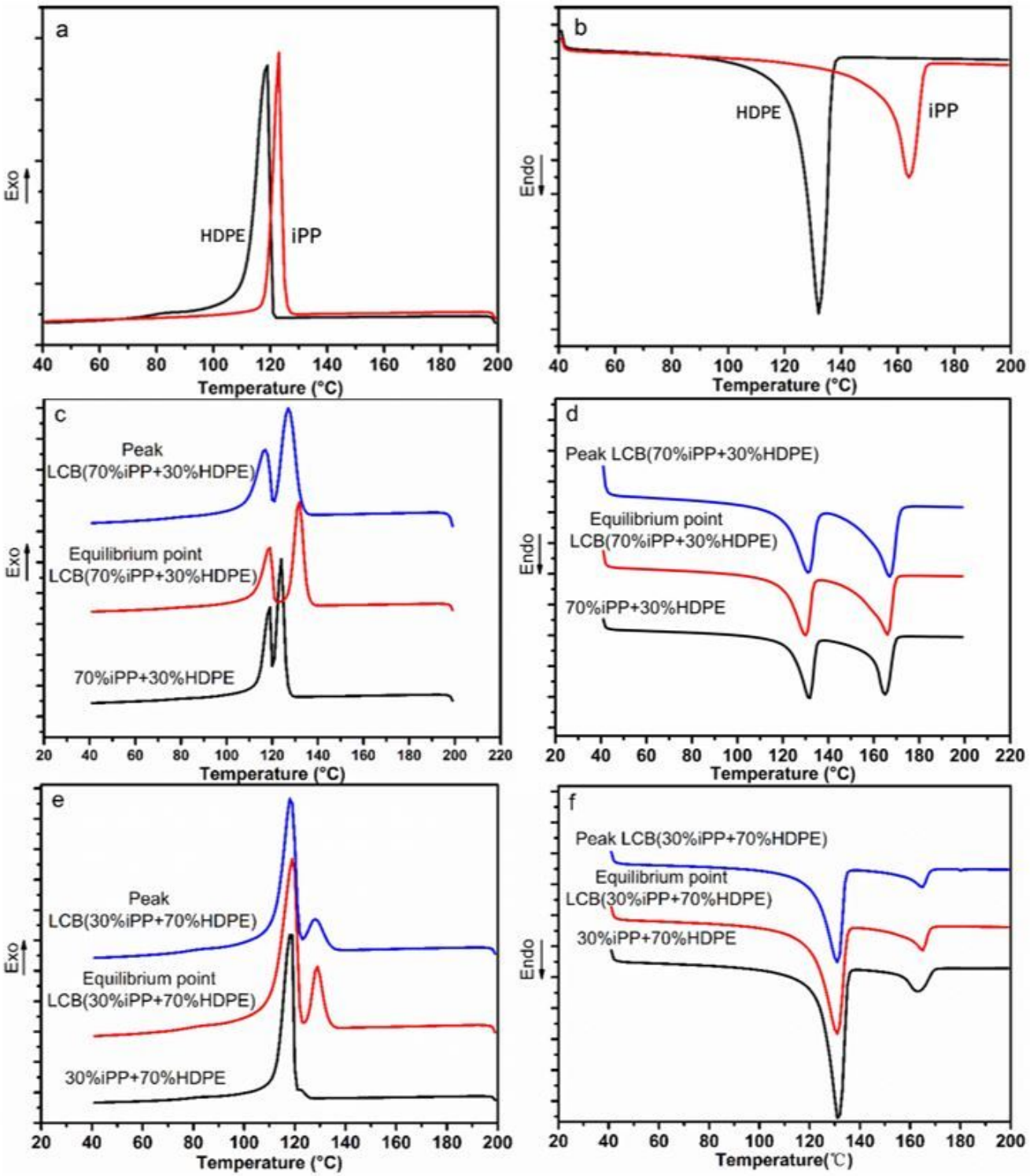

Figure 10

DSC thermograms. (a) Cooling curves and (b) melting curves of HDPE and iPP; (c) Cooling curves and (d) melting curves of iPP/HDPE 70/30 blends; (e) Cooling curves and (f) melting curves of iPP/HDPE 30/70 blends.

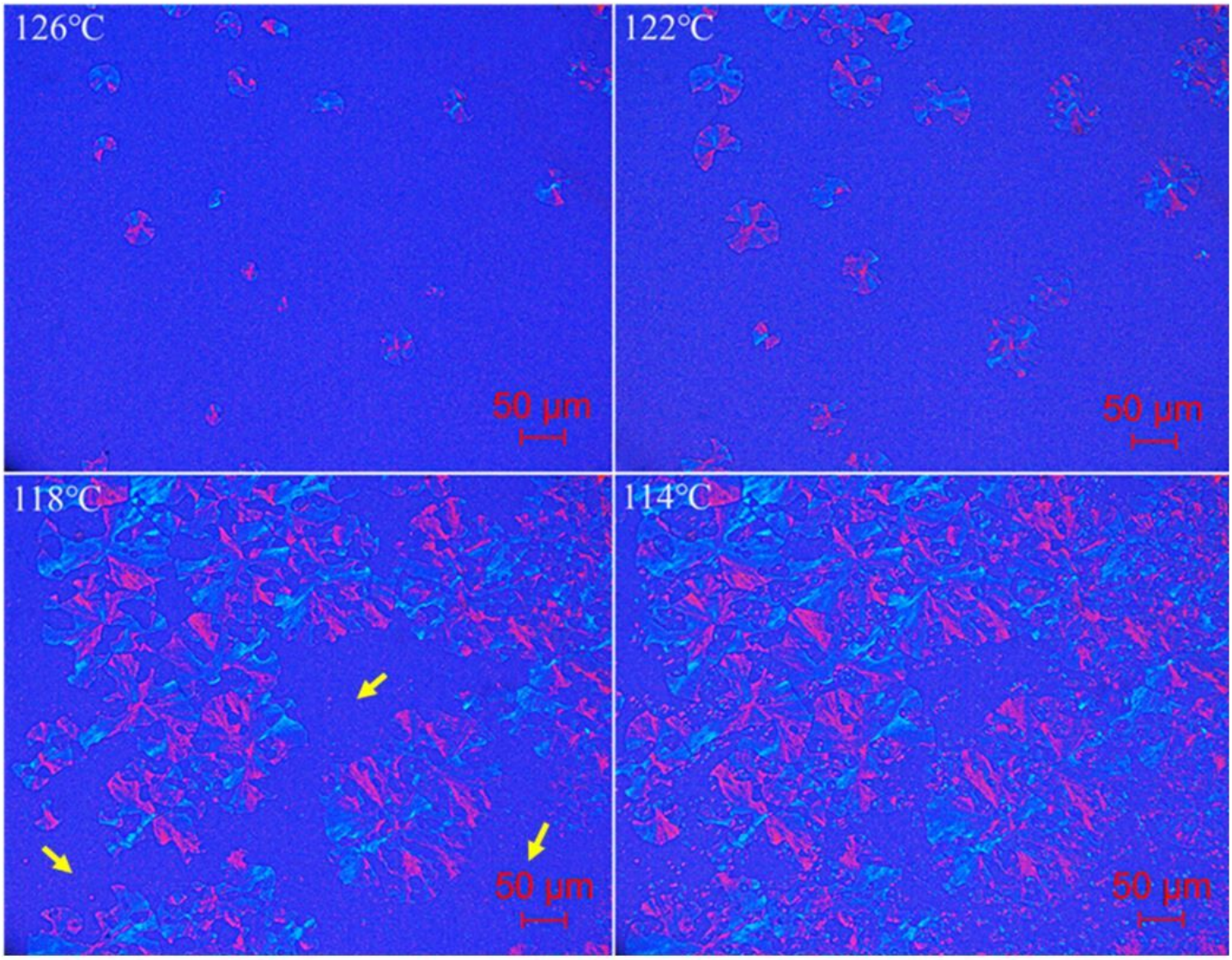

Figure 11

Polarized optical pictures of pure iPP/HDPE 70/30 blend during the crystallization process.

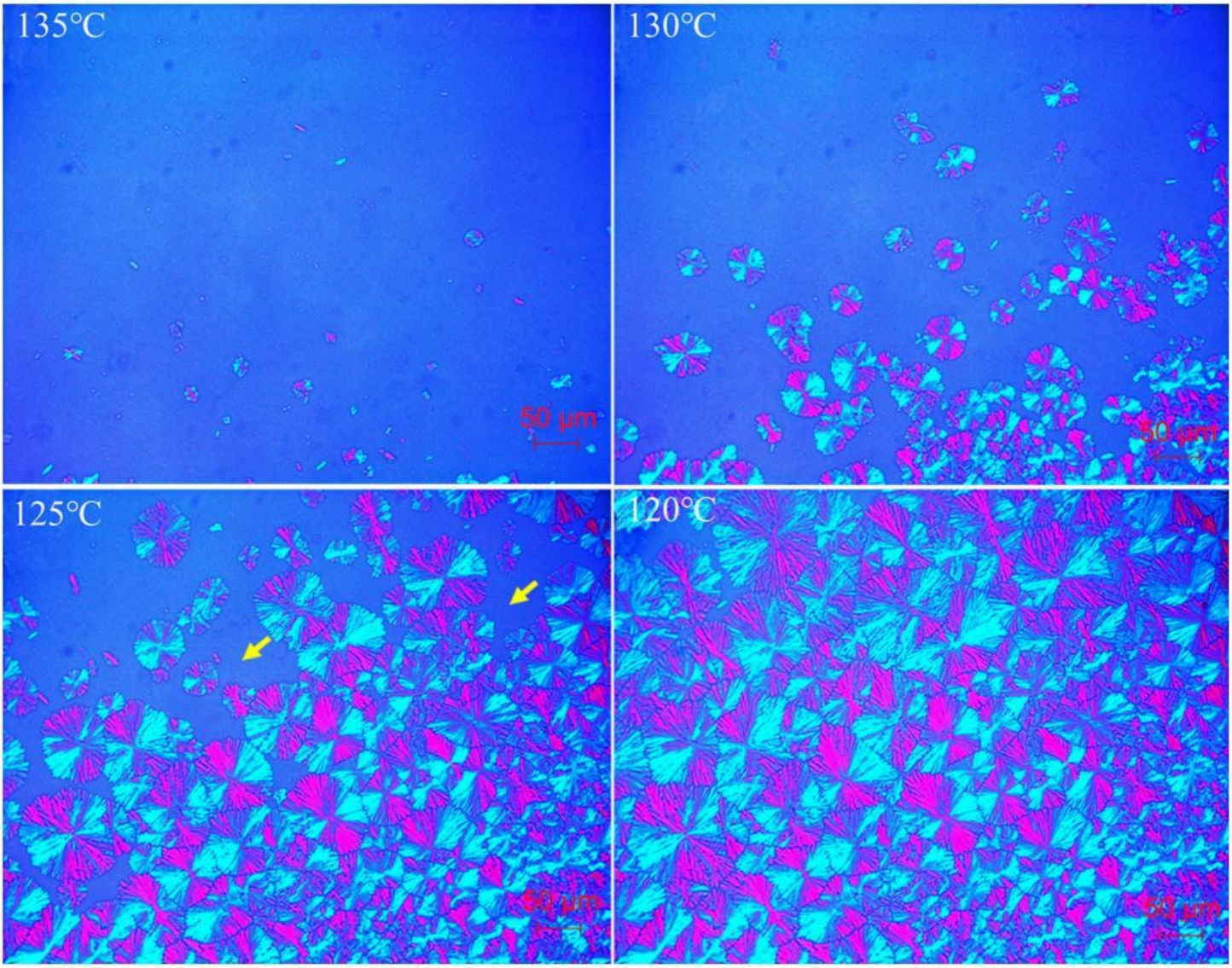

Figure 12

Polarized optical pictures of modified iPP/HDPE 70/30 blend during the crystallization process.

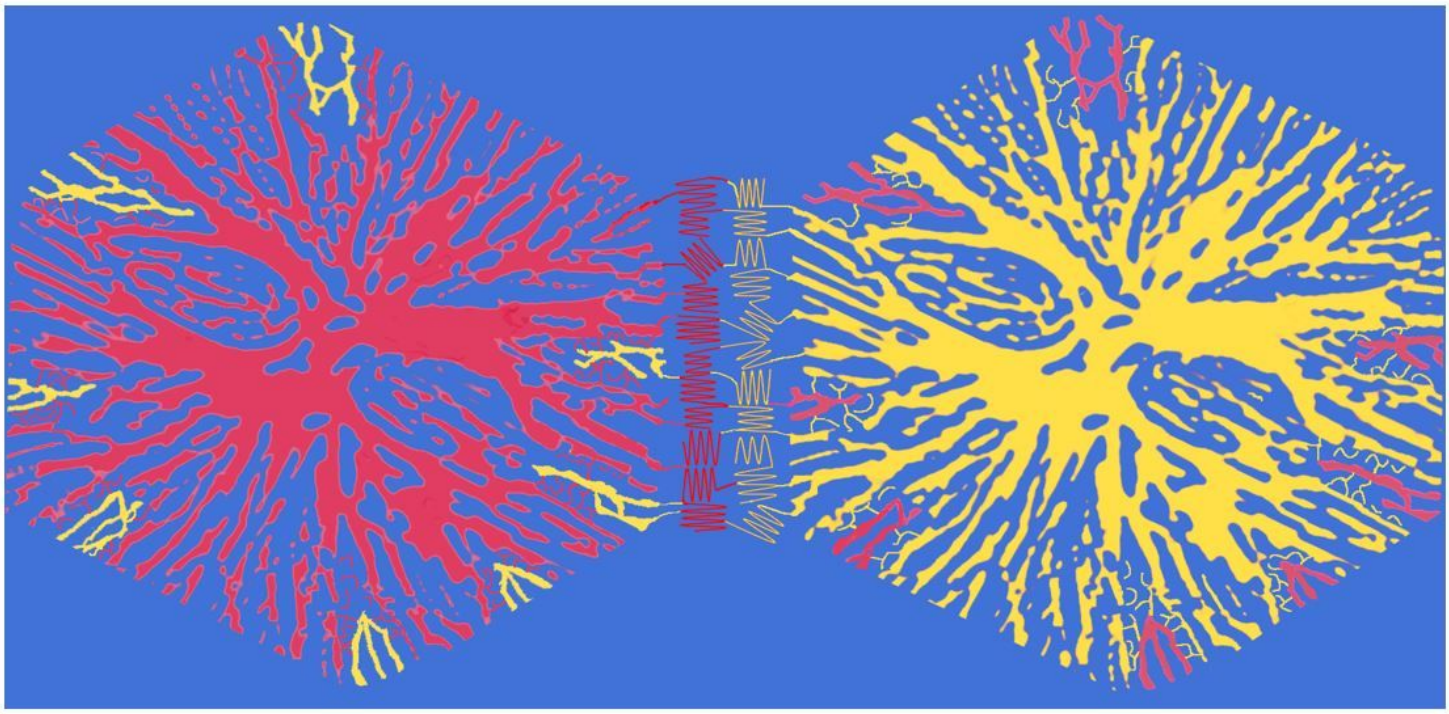

Figure 13

Schematic diagram showing the in situ compatibilization of the iPP/HDPE blend by the LCB copolymer (Red represents iPP, and yellow represents HDPE.).